Journal of Structural Biology 177 (2012) 358–366

Contents lists available at SciVerse ScienceDirect

Journal of Structural Biology

journal homepage: www.elsevier.com/locate/yjsbi

Water's potential role: Insights from studies of the p53 core domain

X. Xu [a,b], Z. Ma [a,b], X. Wang [a], Z.T. Xiao [a], Y. Li [c], Z.H. Xue [d], Y.H. Wang [a,b,*]

[a] Center of Bioinformatics, Northwest A&F University, Yangling, 712100 Shaanxi, China
[b] College of Life Sciences, Northwest A&F University, Yangling, 712100 Shaanxi, China
[c] School of Chemical Engineering, Dalian University of Technology, Dalian, 116024 Liaoning, China
[d] Computer Network Information Center, Chinese Academy of Science, 4th South Street, Zhongguancun, Beijing 100190, China

ARTICLE INFO

Article history:
Received 14 August 2011
Received in revised form 6 December 2011
Accepted 6 December 2011
Available online 14 December 2011

Keywords:
p53 core domain
Hydration
Molecular dynamics
Misfolding

ABSTRACT

Soluble proteins with amyloidogenic propensity such as the tumor suppressor protein p53 have high proportion of incompletely desolvated backbone H bonds (HB). Such bonds are vulnerable to water attack, thus potentially leading to the misfolding of these proteins. However, it is still not clear how the surrounding solvent influences the protein native states. To address this, systematic surveys by molecular dynamics simulations and entropy analysis were performed on the p53 core domain in this work. We examined seven wild/mutant X-ray structures and observed two types of water-network hydration in three "hot hydration centers" (DNA- or small molecule- binding surfaces of the p53 core domain). The "tight" water, resulting from the local collective hydrogen-bond interactions, is probably fundamental to the protein structural stability. The second type of water is highly "dynamical" and exchanges very fast within the bulk solution, which is unambiguously assisted by the local protein motions. An entropy mapping of the solvent around the protein and a temperature perturbation analysis further present the main features of the p53 hydration network. The particular environment created by different water molecules around the p53 core domain also partly explains the structural vulnerabilities of this protein.

1. Introduction

Water's function in the cell is far beyond that of an inert solvent. It is essential for protein structure, which defines the collapse of the hydrophobic core, maintains the stability and structure of proteins, and also drives the folding of proteins by the gain in translational entropy of water molecules bound to the proteins in the unfolded state upon their release (Levy et al., 2006). Despite the simple structure of water and its obvious importance, up-to-date the specific interactions between water and proteins are still poorly understood. In this study, we present a survey of water properties surrounding proteins with a special emphasis on the dynamic role water of the tumor suppressor p53.

The p53 is a tetrameric multidomain transcription factor that activates the transcription of genes in response to cellular stress for cell cycle arrest, senescence, or apoptosis (Vogelstein et al., 2000). In addition to interacting with double-stranded sequence-specific DNA (Ishimaru et al., 2009), the p53 monomer is a modular protein constituted by an N-terminal transactivation domain, a central DNA-binding domain and a regulatory C-terminal oligomerization domain (Okorokov et al., 2009). The p53 core domain (residues 94-312) folds into an antiparallel β-sandwich that coordinates two loops (L2 and L3), which determines the overall stability of the protein (Khoo et al., 2009). Because the domain is inherently unstable and melts at just above body temperature, it is susceptible to oncogenic mutations that inactivate it by lowering its stability (Cañadillas et al., 2006). Experimental studies have shown that this domain is the location of nearly all of the mutations that inactivate p53 in some 50% of human cancers, thus making it an appealing target for cancer therapies (Vousden et al., 2002; Silva et al., 2010).

Interestingly, the p53 mutations which induce misfolding of this protein, can lead to formation of amyloid-like fibrils (Ishimaru et al., 2003); such proteins appear to possess significant populations of nonnative folding states through which the fibers initiate. These insoluble fibrillar polymers in p53 contribute to failure of the expression of a variety of genes leading into uncontrolled cell cycle (Silva et al., 2010), and seed the accumulation of conformationally altered protein. Such disorders include cystic fibrosis disease, inherited emphysema disease, and many types of cancer (Ishimaru et al., 2009).

Recent studies have shown that backbone amide–carbonyl H bonds (HB) are determinants of protein structure when the surrounding water is excluded or highly structured (Fernández et al., 2003). For the disease-related amyloidogenic proteins such as p53, it possesses a high concentration of incompletely desolvated

* Corresponding author at: Center of Bioinformatics, Northwest A&F University, Yangling, 712100 Shaanxi, China.
E-mail address: yh_wang@nwsuaf.edu.cn (Y.H. Wang).

1047-8477/$ - see front matter © 2011 Elsevier Inc. All rights reserved.
doi:10.1016/j.jsb.2011.12.008

backbone HB (Fernández et al., 2003). The segments of such structural 'defects' on p53 are less stable and structurally more vulnerable for misfolding (Fernández et al., 2003, 2004), which gives insights into the relationship between structural instability and misfolding propensity. Combined, a series of important issues have been raised. For example, (1) how does the surrounding solvent influence the native state of p53? and (2) what are the characteristics of the hydration network in the protein?

In this study, we provide an extensive analysis of the p53 hydration supported by MD simulations based on our previous work (Xu et al., 2011a,b), since experimental evidence for the dynamics of solvent at a protein surface is very hard to obtain (Modig et al., 2004). We find that the p53 core domain possesses three "hot hydration centers" (L2, L3 and S7/S8). And two types of waters are also distinguished: the "tight" and the "dynamical" waters. The former probably protects the local folding of p53, and the latter likely influences the fate of this protein prone to misfolding. The temperature perturbation, together with a mapping of solvent entropy around the protein further clarifies the difference between the two types of waters. Our MD simulation studies therefore paint intriguing pictures of the effects of water molecules surrounding the p53 surface at atomic level, which explains why p53 possesses misfolding properties to some extent.

2. Results and discussion

2.1. Distribution of "hot hydration centers" of p53

In order to characterize the solvent spatial probability distributions around the p53 core domain, we have performed time-averaged water density maps for all the MD simulations (De Simone et al., 2005) (Fig. 1). With the MD hydration sites identified as local maxima in the density function, we compare the density distribution for water oxygen atoms in seven different simulations of the p53 structures (PDB codes: 2OCJ, 1UOL, 2J1Y, 2QVQ, 2WGX, 2X0U and 3DO5, all these proteins are free p53 core domain), and find a good consistency among the hydration regions (Fig. 1 and supporting information S1–S5). The spatial distribution of hydration sites is generally anisotropic and asymmetric, showing regions where the hydration sites are tightly clustered and regions that are almost devoid of sites. For further verifying the overall structure of the hydration shell observed in the simulations, we compare the hydration sites determined by the 20 ns MD simulations with those detected by the X-ray crystallography. The results show that of the water molecules detected by the two techniques, only about 25% fall at same sites. However for MD hydration sites with a long residence time (residence time (τ) > 2.5 ns), the discrepancy between the simulated and crystals sites is strongly decreased, and shows a very well agreement, indicating that these are conserved waters. Many short residence times (τ < 2 ns) for waters in p53 hydration layers are also observed, showing a poorer correlation with the solvent structure in X-ray.

Further observation of the MD water-density regions in p53 (PDB ID codes 2OCJ and 1UOL) shows that the high density regions are mainly distributed around the hot centers L2 (residues Tyr163–Ile195), L3 (residues Tyr236–Ile251), and S7/S8 turn (residues Pro219–Thr230), while the low density areas are mainly located in β-sheets which provide the basic scaffold for the DNA-binding surface (Okorokov et al., 2009) (Fig. 1). The results indicate that L2, L3 and S7/S8 possess at least three parts (residues Leu188–Ile195 in L2, Asn239–Gly245 in L3, and Asp228–Thr230 in S7/S8) protected by the highly structured waters (Papoian et al., 2004).

Moreover, a superposition of the seven structures (root-mean-square deviations (rmsds) of 2.99 Å) reveals that the major structural variations also occur in the three hot areas (Kitayner et al., 2006). This implies the structural mobility of L2, L3 and S7/S8, and the lack of protection of the backbone HB (Fernández et al., 2004) on the surface of their certain regions. Since the incompletely dehydrated backbone HB makes a soluble protein reliant on binding partnerships for the preservation of its fold (Fernández et al., 2003), the two loops and the strand should be the putative epitopes for the ligand binding. Indeed, experimental studies have identified L2 and L3 as the DNA-binding surface via the direct interactions between Gln165, His168, Arg249 and DNA, and S7/S8 as the surface for the binding of small molecules (Okorokov et al., 2009; Basse et al., 2010; Cho and Y., 1994; Wasielewski et al., 2006). Interestingly, after checking the water behavior surrounding Gln165, His168, Arg249 in all the systems, we find that there is no any highly structured water adjacent to these residues (distance <3.5 Å), but only motional waters. This suggests when DNA binds to L2 and L3, the motional waters on their surface are excluded, and DNA acts as an alternative to protect the local structure of p53 (Fernández et al., 2003).

In this section, we thus suggest that the core domain of p53 possesses three "hot hydration centers" located at the L2, L3 and S7/S8, respectively. For the sake of clarity, we refer the three hydration parts (Leu188–Ile195 in L2, Asn239–Gly245 in L3, and Asp228–Thr230 in S7/S8) with backbone HB well-protected as to "regions

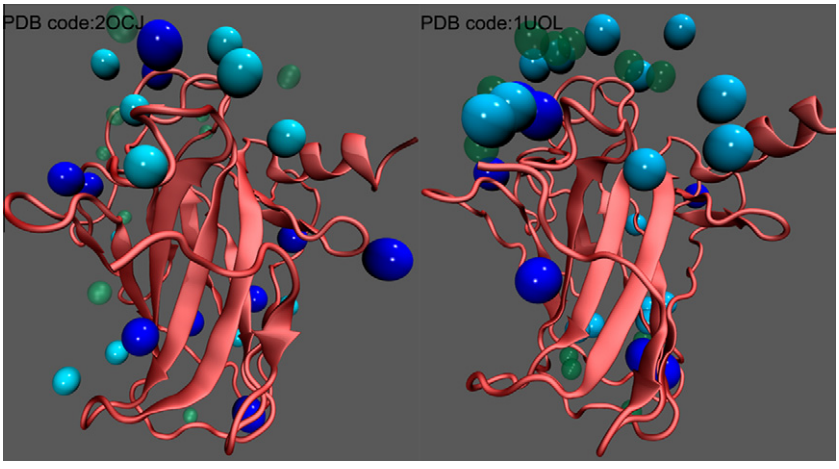

Fig.1. Three-dimensional distribution of high-density solvent around p53 with the p53 structures (PDB code: 2OCJ and 1UOL) as the reference structures. In the solvation map, hydration sites with low (1 < τ < 2 ns), medium (2 < τ < 2.5 ns) and long (τ > 2.5 ns) residence times are colored green, cyan and blue, respectively. (For interpretation of the references to color in this figure legend, the reader is referred to the web version of this article.)

A, B and C", respectively (Fig. 2). Meanwhile, we also establish a base line to specify the water molecules. For the waters that occupy the hydration sites with relatively long residence time, we refer them as "tight" waters. While the waters that are localized in the hydration sites with temporal residence time and feature high mobility, are defined as "dynamical" waters. In addition, it should be noted that the MD simulation can be coupled with continuum mechanics to describe the behavior of waters that is approximated as continuous for time scales. Thus in this paper, the categorization for waters is actual an extreme approximation of the continuum of time scales sampled.

2.2. "Tight" water molecules

Table 1 presents the highest MD residence time calculated for waters in the three regions (A, B and C) that are determined in all of the available X-ray structures. It should be noted that water occupancy is not well correlated to the residence time. For the sites of high occupancy, they can also have low residence times for any individual molecule. As shown in this table, there is a large discrepancy from these residence times and the ones calculated on the maxima of the MD water density. These waters are all exposed and correspond to some of the structurally conserved X-ray waters; their structural features are described in details as below.

2.2.1. Hydration sites in the region A

For region A, it has an average residence time of 2.5 ns, and processes two hydration sites: a1 and a2 (Fig. 3A). Both sites have corresponding water molecules in the X-ray structures (Table 2). If we plot the two hydration sites in a graph, we get a straight line through the points with a distance of ~6.0 Å which almost parallels to β-sheet 5. a1 connects L2 and β-sheet 5 that are separate in spatial distribution and belong to different secondary structural elements. This water bridges the Ala189, Pro190 and His193 backbone oxygen (Fig. 3a1). The water molecule is locked in the site in four simulations including the wide-type (2OCJ) and the mutant (2QVQ, 2WGX and 3DO5) systems. While in the 1UOL, 2J1Y and 2X0U systems, the site a1 is changed into site a2, which is caused by slight displacements of the Pro190 and His193 residues in this region, thus impeding the restructuring of the water. The site a2 is located at the end of L2, and only involves an H-bond with the amino hydrogen of Gln192 (Fig. 3a2). Since Gln192 makes a tight contact with Arg181, a key residue to interact with DNA (Ma et al., 2007), we imply that the conformational change of Gln192 is able to interfere with the specific binding to some extent. The binding free energies of the water molecules in the sites a1 and a2 are −22.21 and −22.05 kJ/mol, respectively. This result shows that the waters are bound with similar energies in the region A, and provides an estimation of the local stabilization due to the protein–water interactions.

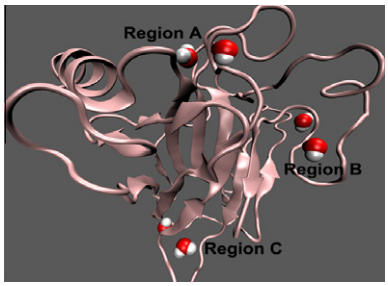

Fig.2. The distribution model of the hydration sites a1 and a2, b1 and b2, and c1 and c2 in the regions A, B and C, respectively.

Since the waters in the sites a1 and a2 have relatively long residence time and form stable HB with their surrounding residues, we propose that these waters probably stabilize the region A, thus maintaining the general framework of the protein. This implies that the structured waters are still capable of maintaining the correct folding of region A even with slight displacements of their ambient residues (Pro190 and His193). Unfortunately, we cannot remove the sites a1 and a2 waters from the region A (on the surface of p53) to prove that these waters are definitely essential in stabilizing the local conformation of p53.

Despite of that, recent MD simulations have still provided deep insights into the coupled water–protein motions although quantitative discrepancies exist (Zhang et al., 2009). For example, four snapshots from the trajectory of MD simulation (PDB code: 2OCJ) for the site a1 of region A reveal that accompanied by the motions of protein, the nearby hydration water proceeds to local orientational and slight translational motions (Fig. 3B). Subsequently, the water network makes small structural arrangements, and meanwhile the hydration water (Sol) 231 dynamically exchanges with bulk water in tens of picoseconds. The new Sol 1147 immediately occupies the site a1 at 16.5 ns to interact with the backbone oxygen of Ala189 and Pro190, resulting in a net entropy gain for Sol 231 and the continuing stable folding state of the protein. This intimate coupling is actually a direct reflection of local water motions, implying the contribution of stable hydration sites for the possible stability of the protein.

2.2.2. Hydration sites in the region B

Region B also contains two hydrations sites (b1 and b2); linking of such two sites results in a line with a distance of ~6.5 Å, almost parallels to β-sheet 10 (Fig. 4A). We find that even the poorer identified MD hydration site b2 would have at least two corresponding water molecule in the seven X-ray structures (Table 2). Site b1 has been located in the wild (2OCJ) and mutant (1UOL, 2J1Y and 2QVQ) systems, and is positioned between the end of the β-sheet 10 and the L3 segment. Its adjacent site b2 has resided in the 2WGX and 3DO5 systems, and is sandwiched between β-sheets 9 and 10. Both sites are enclosed by residues Asn239, Ser240, Arg249, Val272, Arg273 and Val274 that are solvent-exposed or well-buried on the DNA-binding surface of p53. During the simulations, the region B has much longer residence time (5 ns) than region A, which indicates the presence of stable H-bond networks in this region. Indeed, the sites b1 and b2 are well defined in almost all available p53 structures (Table 2). These calculations reflect the water -mediated interaction of site b1 between the backbone amino of Ser240 and the backbone oxygen of Val274, and that of site b2 between the backbone oxygen of Ile251 and Val272 (Fig. 4 a1 and a2). Experimental studies have reported that substitution of Val272 by methionine specifically prevents p53 accumulation and activation after DNA damage (Barnas et al., 1997), which emphasizes the "hot" position of Val272 and the importance of site b2. Evidently, both sites bridge the β-sheet 10 and L2 where the DNA-binding residues Arg249 and Arg273 are located, indicating that the flexibility of β-sheet 10 and L2 may be affected by the strength of the water-mediated H-bonds. For the region B, the free energies of binding for sites b1 and b2 are −23.20 and 23.70 kJ/mol, respectively, and the binding energies are enhanced ~1.5 kJ/mol compared with those in the region A. Indeed, the protons from the waters in the two sites are likely to be strongly coupled magnetically to the cluster in region B as the protons are 2.0 and 2.7 Å from Val274 and Val272, respectively. These results evidently imply the important roles of the hydration sites surrounding the region B.

Figure 4B shows four snapshots from the trajectory of MD simulation (PDB code: 2OCJ) for the site b1 of region B. At time 16.6 ns, there are conformational rearrangements arising from the local motions of the water network nearby residue Ser240 that leads

Table 1
Highest residence time of the X-ray conserved waters in the regions A, B and C.

Region	Site	2OCJ	1UOL	2J1Y	2QVQ	2WGX	2XOU	3DO5	τ (ns)
A	a1	1147	–	–	2444	2794	–	5603	1.5
	a2	–	2650	5603	–	–	8907	–	3.0
B	b1	4491	4829	1298	3989	6972	–	–	8.0
	b2	–	–	–	–	5930	–	940	2.0
C	c1	465	6413	1262	–	–	6512	1027	14.0
	c2	–	–	–	6932	5211	–	–	2.5

The seven center rows are described by PDB ID codes, and the water numbering in each PDB file is recorded.

to dynamical exchanges with bulk water. The cooperative motions result in the replacement of the original water molecule Sol 7133 in site b1 with the bulk water Sol 4491, and the hydrating water consequently reaches the equilibrated configuration, i.e., the site b1.

2.2.3. Hydration sites in the region C

Region C is comprised of two hydration sites with a distance of 6 Å: sites c1 and c2 (Fig. 5A). The water in site c1 interacts with the backbone carbonyl and hydrogen of two vicinal residues (Asp228 and Thr230) in strand S7/S8 (Fig. 5a1). This hydration site is present in the 2OCJ, 1UOL, 2J1Y, 2X0U and 3DO5 systems and is replaced of the site c2 in the remaining systems, where it interacts only with Val147 in the S7/S8 (5a2). Both of the hydration sites are sited neighboring to the S7/S8 strand that is rigid in all simulations (RMSF is ~0.95 Å for residues Pro219–Thr230). This result indicates that this strand remains stable and hydrated during the simulations. The calculated water-binding free energies are −22.21 and −22.05 kJ/mol for sites c1 and c2, respectively, very similar to sites a1 and a2 in the region A. Additionally, as shown in Fig. 5, the water network nearby residues Asp228 and Thr230 proceeds to structural arrangements, and at this moment (at 2.7 ns), the water molecule Sol 1465 from the bulk water occupies the site c1 of region C. The coupled interactions between the water and the

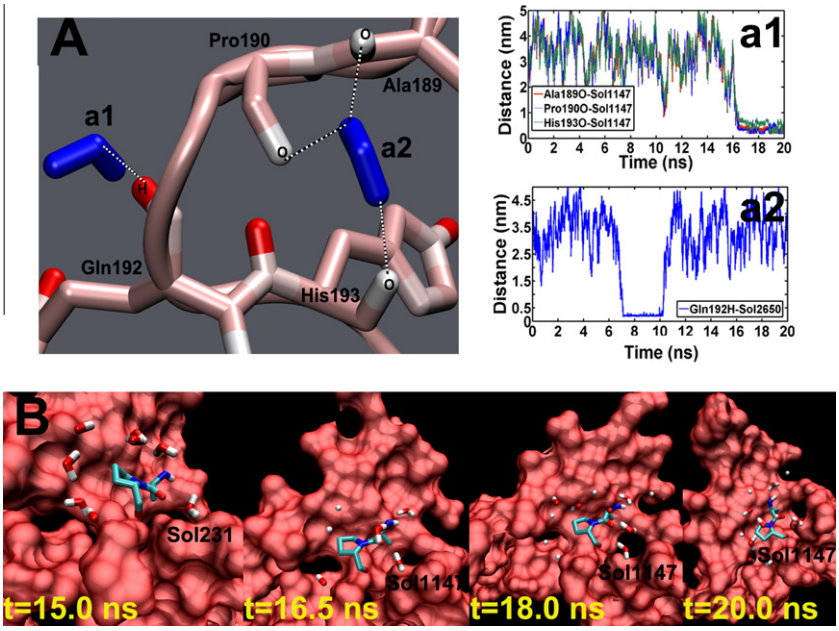

Fig.3. (A) The close-up view of the hydration properties of region A in the loop L2. (a1) Time evolutions of the distance between Ala189–O, Pro190–O, His193–O and water molecule Sol 1147 in the MD simulation (PDB code: 2OCJ), respectively. (a2) Time evolution of the distance between Gln192-H and Sol 2650 in the representative MD simulation (PDB code: 1UOL). (B) Snapshots of water motions with the MD trajectory of 2OCJ. Depicted here is the site a1 of region A with residues Ala189 and Pro190 shown in stick presentation. The water molecules within 3.5 Å from the two residues are shown in stick. At time 16.5 ns, the Sol 1147 from the bulk water interacts with the backbone oxygen of Ala189 and Pro190 to displace Sol 231 in site a1.

Table 2
H-bond distance (Å) between water molecules and protein residues in the X-ray structures.

Region	Site	Atom	2OCJ	1UOL	2J1Y	2QVQ	2WGX	2XOU	3DO5
A	a1	Ala189-O	4.04	–	–	4.42	4.49	–	4.49
		Pro190-O	2.03	–	–	3.22	2.22	–	2.22
		His193-O	3.28	–	–	2.24	2.71	–	2.71
	a2	Gln192-H	–	2.98	1.98	–	–	4.12	–
B	b1	Ser240-HG	1.98	2.03	1.59	–	2.00	–	–
		Val274-O	–	3.34	2.47	2.37	4.56	–	–
	b2	Ile251-O	–	–	–	–	4.06	–	4.49
		Val272-O	–	–	–	–	3.03	–	3.02
C	c1	Asp228-O	2.50	3.87	2.27	–	–	3.70	4.68
		Thr230-H	5.75	2.90	4.31	–	–	2.73	2.90
	c2	Val147-H	–	–	–	1.94	2.08	–	–
		Val147-O	–	–	–	3.49	2.82	–	–

The right seven rows are described by PDB ID codes.

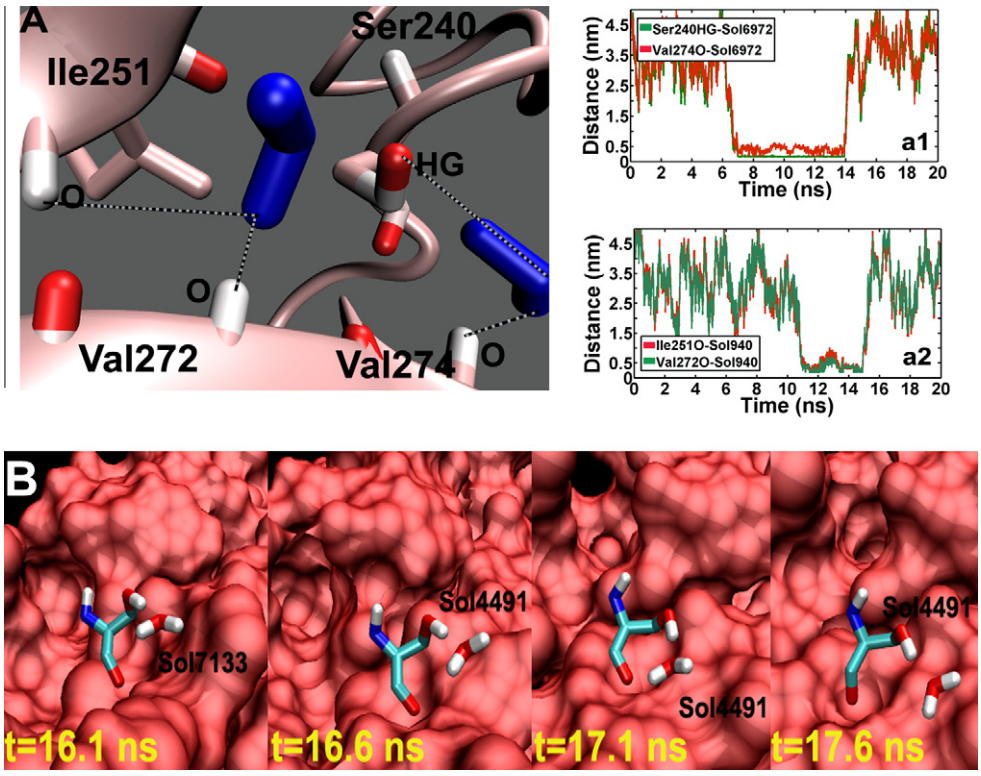

Fig.4. (A) Hydration properties of region B of p53. (a1) Time evolutions of the distance between Ser240–HG, Val274–O and Sol 6972 in the representative MD simulation (PDB code: 2WGX), respectively. (a2) Time evolutions of Ile251–O, Val272–O and Sol 940 in the representative MD simulation (PDB code: 2WGX), respectively. (B) Snapshots of water motions around the site b1 of region B with the MD trajectory of 2OCJ. Residue Ser240 is shown in stick presentation. At time 16.6 ns, the Sol 4491 from the bulk water interacts with Ser240 (HG) to displace Sol 7133 in site b1.

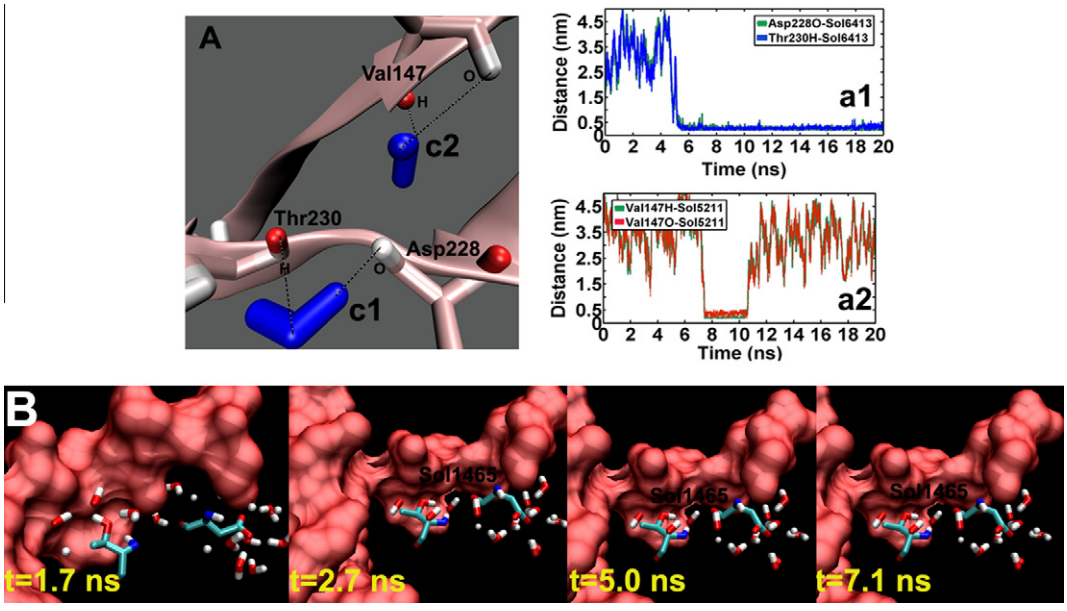

Fig.5. (A) Hydration properties of region C of p53. (a1) Time evolutions of Asp228–O, Thr230–H and Sol 6413 in the representative MD simulation (PDB code: 1UOL), respectively. (a2) Time evolutions of Val147–H, Val147–O and Sol 5211 in the representative MD simulation (PDB code: 2WGX). (B) Snapshots of water motions around the site c1 of region C with the MD trajectory of 2OCJ. Residues Asp228 and Thr230 are shown in stick presentation. At time 2.7 ns, the Sol 1465 from the bulk water interacts with Asp228 and Thr230 and lasts ~4.4 ns.

protein lasts ~4.4 ns, probably protecting the local conformation of the protein p53.

In this section, Table 2 lists the water–protein interactions of regions A, B and C in all of the systems. The various X-ray structures and hydration sites in MD show high consistency despite slight differences among them, such as Ala189–O in PDB code 2OCJ, and Asp228–O in PDB code 1UOL. We find that the main reason for the difference between the simulated and crystal

hydration sites is the absence of the crystal packing effects in the simulation of the protein in solution (Makarov et al., 2000). For the MD simulations, almost no constraints are imposed to the p53 motions although lattice contacts can interrupt the structural and molecular motions to some degree (De Simone et al., 2005).

2.3. "Dynamical" water molecules and their scattered behavior

In the above section, we have identified the "tight" waters in the regions A, B and C, and find that these structured waters have relatively long residence time and enable to form stable HB with surrounding residues. Since p53 is an amyloidogenic protein that is vulnerable to water attack, this implies that there should be at least another type of water around the neighborhood of the protein that is of a different character compared with the "tight" waters. We have therefore mapped the solvent entropy for elucidating the properties of waters, and distinguishing the new type of waters from the "tight" waters. It is worthwhile to note that the solvent entropy map was calculated using the Shannon entropy, with the purpose of measuring the information, choice, and uncertainty of a discrete information source. We use this type of entropy as a way to assign a score to the different regions of p53 that reflects the variability of water distribution in those regions. For the waters forming stable HBs with the P53, we suggest that these "tight" waters are certain and have weak entropy. While for waters with highly dynamical behaviors, we thus propose that they are uncertain and possess strong entropy. Meanwhile, another thing to remember is that the Shannon entropy is different from thermodynamic entropy. The latter is measured in terms of the changes the system has undergone from the previous state to the final state, which is based either on the thermodynamic theory or on harmonic or quasi-harmonic dynamics.

Fig. 6 show the spatial distribution of the entropic potential with blue contours around the C-terminal (region A) and the middle (an unprotected region) of L2. By focusing on the C-terminal of loop 2 (Fig. 6A), we find that the solvent entropy becomes stronger with the increased distance, and in close proximity to the protein surface, forms empty adjacent space. This is reasonable since the "tight" waters adjacent to the protein surface form stable HB that exhibit a certain state, while the entropy signifies a simple quantitative of uncertainty (Helms et al., 2007). When the distance between the waters and the protein surface gradually increases, the waters become more and more dynamical due to the loss of the intermolecular HBs and thus present an uncertain state, which finally leads to the strong entropy. A different picture emerges from the middle of L2 surrounded by waters composed of low-density clusters (Fig. 6B), showing that even around the region in the neighboring of L2 surface, there is still strong solvent entropy. This indicates that the sporadic water exchange leads to an entropy increase.

In addition, the quantitative evaluation of the entropy has shown the similar results (Fig. 6a1 and b1). The C-terminal of L2 with the localized waters represents several large solvation humps around the protein surface and a gradual increase in entropy, whereas the middle of L2 with the mobile waters reveals a steep and prompt increase in entropy. Obviously, the solvent entropy draws a clear dividing line between the "tight" and the "dynamical" waters, and implies the scattered state of mobile waters around the protein.

For increasing the understanding of the solvent behavior in the protein surface, we further analyze water exchanges by evaluating the time evolution of the interacting water with residues around the p53 surface. There are several intraloop hydrogen bonds in the L2, L3 and S7/S8 regions, such as H-bonds between Tyr239 and Ser241 in L3, and between Glu224 and Gly226 in S7/S8 (Figs. 7). Fig. 7a1 and b1 shows the distribution profile of waters in the two regions with their residence times presented by the length distribution, indicating that there are remarkable differences in the water numbers and the residence time between the regions. For the protected region in L3, it is surrounded by hydrations sites with medium residence times, and processes only a limited number of waters that interact directly with the Tyr239–Ser241 H-bond. While for the unprotected region in S7/S8, its intensive scattered plot shows a very fast water exchange, and relatively shorter residence times of waters compared with the times observed in the protected region.

3. Temperature perturbation for p53

Recent study has shown that the core domain of p53 enable to form fibrillar aggregates after a mild temperature treatment (Ishimaru et al., 2009). On the basis of the thermodynamical property of p53, we would like to explore the water behavior after the use of temperature as a perturbation technique to interfere the native state of p53.

Here, we choose four temperatures for the MD simulations of wild and mutant p53 (PDB codes: 2OCJ and 1UOL): 36, 39, 42, and 45 °C, which are converted from 310, 312, 315, and 318 K for easier understanding. At higher temperatures (42 and 45 °C), we find that the temperatures induce large dynamical transitions of p53, and no "tight" waters appear in the regions A, B and C. While at lower temperatures (36 and 39 °C), almost all the sites in the regions can be found in the two systems except for the sites a1 and c1 at 39 °C. The most likely cause of the difference between the higher- and lower-temperature properties is the disruption of hydration sites induced by the high temperature, which therefore probably destabilized the protein. In order to further observe the solvent behavior with the increase of temperature, we focus on analyzing the solvent-backbone H-bond exchanges around the residues Tyr239 and Ser241 in L3. The plotted maps in Fig. 8 show that the water points (blue) disperse more broadly and homogeneously with the increasing temperature, which indicates faster water exchanges at higher temperature.

4. Conclusions

In this study, we have uncovered the p53 hydration patterns with MD simulations, which identify three regions (A, B and C) in the protein. In each of the regions, there are two stable hydrations sites with a distance of ~6.0 Å, which probably facilitate stabilizing the protein.

The distribution maps of the solvent entropy in the protected and unprotected regions show a 'dual-behavior' of water surrounding the protein surface. Such a behavior is reminiscent of the close association between the properties of waters and the entropy distribution: When the clustered water molecules occupy the hydration sites, the solvent entropy adjacent to the protein surface becomes weaker, and forms a protection strip to separate protein surface and bulk solvent. Whereas the presence of high mobile waters induces the vast distribution of entropy in the protein, even extremely close to the surface. These results indicate that the free energies derived from the water-backbone H-bonds are equivalent to the maximizing solvent entropy during the folding.

Moreover, the research for the water behaviors around the p53 protein has explained the dynamical mechanism of the formation of the misfolded conformation to some extent, which may ultimately facilitate exploring the suppression mechanism of tumor development.

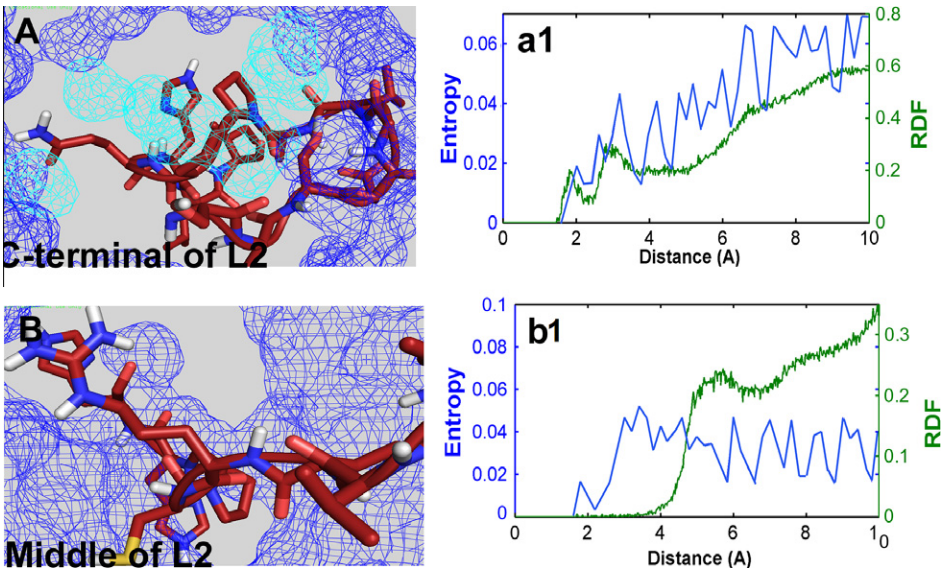

Fig.6. The entropy-based water distribution map of the C-terminal (A) and the middle (B) of L2. The blue grids represent the high entropy regions, and the cyan grids are the hydration sites around the protein surface. The C-terminal and the middle of L2 is colored in red, and the residues are shown in stick representation. (a1) shows the double coordinate system of entropy vs. distance and radial distribution function vs. distance surrounding the C-terminal of L2. The entropy (blue) represents several large humps, but a gradual increase. And the radial distribution function (green) shows a relatively smooth curve. (b1) shows the double coordinate system of entropy vs. distance and radial distribution function vs. distance in the middle of L2. Both the entropy and the radial distribution function curves present a steep increase at the beginning. (For interpretation of the references to color in this figure legend, the reader is referred to the web version of this article.)

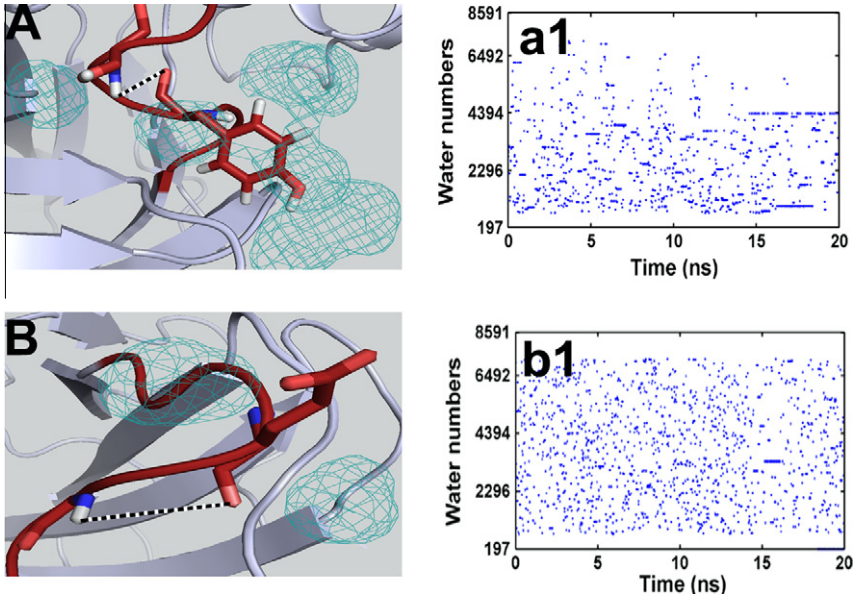

Fig.7. The distribution profile of "tight" (A) and "dynamical" (B) waters. (A) shows the H-bond between Tyr239 and Ser241 in L3, as shown by the dashed line. The cyan contours represent the water molecules around the protein surface. (a1) shows the time evolutions of each water within a distance of 2.5 Å around the surface of L3. The length of lines represents the residence times of the waters. (B) shows the H-bond between Glu224 and Gly226 in S7/S8. (b1) shows the time evolutions of each water within a distance of 2.5 Å around the surface of S7/S8.

5. Methods

5.1. Simulation systems

In this study, we focused on the solvent behavior surrounding the p53 surface. Initial coordinates for the monomeric systems were taken from all the available X-ray crystal structures of wild-type (PDB ID code 2OCJ) and mutant-type (PDB ID codes 1UOL, 2J1Y, 2QVQ, 2WGX, 2X0U and 3DO5) p53 proteins. The missing hydrogen atoms, main chains, and side chains in the crystal structures were reconstructed by using the DeepView/Swiss-PdbViewer 3.7 software (Guex et al., 1997). The spatial environment of each new residue was checked for close contacts or overlaps with neighboring residues, and stereochemical regularization of the structures was obtained by the Powell minimization method implemented in the Deepview program. All simulations were performed using GROMACS 4.0.4 package (Berendsen et al., 1995), with the Gromos96 force field (Daura et al., 1998). A cubic box of TIP3P water was used (Jorgensen et al., 1983), keeping a minimum distance of 12 Å between the solute and each face of the box.

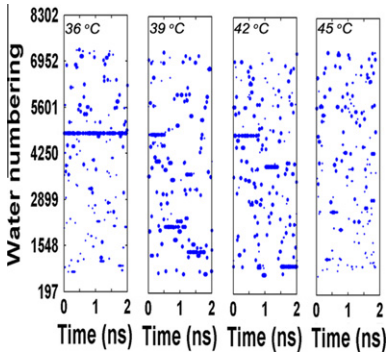

Fig.8. Distribution profiles of waters (blue points) around p53 with the temperature as a perturbation technique to interfere the stability of the protein (36, 39, 42, and 45 °C). The waters disperse more broadly and homogeneously with the increasing temperature, which indicates faster water exchanges at higher temperature. The length of lines represents the residence times of the waters. (For interpretation of the references to color in this figure legend, the reader is referred to the web version of this article.)

All systems were first optimized using the 5000 steps of steepest descent and 10,000 steps of conjugate gradient minimizations. Then the solvent molecules in the minimized models were heated up to 300 K and equilibrated 200 ps with the positional restraints on the protein heavy atoms by using a force constant of $k = 1000\ \mathrm{kJ\ mol^{-1}\ nm^{-2}}$. All simulations were performed in the NTP ensemble at constant pressure (1 atm) with isotropic position scaling and at 300 K with the Berendsen temperature coupling $T_p = 0.1$ ps. The pressure was coupled to a Berendsen barostat with $T_p = 0.5$ ps and an isotropic compressibility of $4.5 \times 10^{-5}\ \mathrm{bar^{-1}}$ in the *x*, *y*, and *z* directions (Berendsen et al., 1984). The integration time step was 1 fs with all bonds constrained according to the LINCS algorithm (Hess et al., 1997). Short-range van der Waals energy was truncated at 14 Å. Electrostatic interactions were calculated with the particle mesh Ewald method (Darden et al., 1993) employing a grid spacing of 0.12 nm to achieve an accurate and efficient treatment of the long-range electrostatic interactions. Finally, a series of nine 20 ns MD simulations were generated for the p53 protein. The coordinates of the simulations were written out every 5 ps for subsequent analysis.

5.2. Water density analysis

The solvent density map from the MD trajectory was estimated from the water oxygen atom positions as described by Lounnas and Pettitt (Lounnas et al., 1994a,b). The MD hydration sites are assigned as the local maxima of the function, following the restrictions to be the highest value in a radius of 0.14 nm with a minimum density of 1.7 times the value of bulk water. The space surrounding the protein is divided in two shells: the first region describes the water within a distance of 0.6 nm from the protein surface. The second region goes from 0.6 to 0.8 nm from the protein surface and represents the bulk solvent shell. The density function is grid based (step-size 0.05 nm). The atom coordinates were transformed by superimposing the protein conformations in the trajectory onto a reference model. Based on these, the water distribution map was obtained.

5.3. Binding free energy

The binding free energy of water molecules buried in cavity of protein is calculated by the double decoupling method (Hamelberg et al., 2004). Two steps are involved: (1) calculation of the free energy for decoupling the water molecule of interest from the binding site of p53 (ΔG_1°); (2) calculation of the free energy cost of decoupling a water molecule from bulk solvent to gas phase (ΔG_2°). As shown in the following formulas, reaction (1) is the "annihilation" of the water molecule B from the solvated p53-water complex AB. Reaction (2) is the "annihilation" of the water from solvent. The free energy change of the two reactions, ΔG_1° and ΔG_2° yields the absolute free energy of binding, ΔG_{AB}°:

$$AB(\mathrm{sol}) \rightarrow A(\mathrm{sol}) + B(\mathrm{gas}) \quad \Delta G_1^\circ \tag{1}$$

$$B(\mathrm{sol}) \rightarrow B(\mathrm{gas}) \quad \Delta G_2^\circ \tag{2}$$

$$A(\mathrm{sol}) + B(\mathrm{sol}) \rightarrow AB(\mathrm{sol}) \quad \Delta G_{AB}^\circ = \Delta G_2^\circ - \Delta G_1^\circ \tag{3}$$

ΔG_2° is independent of the standard concentration. The calculation of ΔG_1° is straightforward and can be computed by thermodynamic integration as shown in Eq. (3) or by a free energy perturbation approach.

$$\Delta G_{AB}^\circ = \int_{\gamma_B}^{\gamma_A} \frac{dG}{d\lambda} d\lambda \tag{4}$$

MD simulations were performed in parallel for all steps along the decoupling pathway in this study with GROMACS 4.0.4 package using all parameters in the above section.

5.4. Measurement of water exchange rate

The water exchange rate (residence time) in the hydration site is calculated by the time-autocorrelation function $p(\tau)$ Lounnas et al., 1994b, shown as follows:

$$p(\tau) = \sum_t \delta(W(t), W(t+\tau)), \tag{5}$$

where the function $\delta(W(t), W(t+\tau)$ is 0 or 1, respectively, whether or not the indexes of the waters residing in the hydration site at times t and $t+\tau$ differ. An exponential model is applied further to fit the resulting time-autocorrelation function.

5.5. Solvent Entropy

In order to understand how the spatial distribution of the solvent around the protein affects the state of hydration sites, the solvent entropy map was calculated using the Shannon entropy. The solvent entropy map was computed in 0.1-nm-spaced circle, each boundary of which was connected to a narrower ring of 0.02-nm mesh size, which takes into count of the water distribution around the ring. The solvent entropy for a generic node of the map is calculated as follows:

$$S = -R \sum_{j,k,l} P_{j,k,l} \ln P_{j,k,l}, \tag{6}$$

where $P_{j,k,l}$ is the probability of finding a water in the subvolume *l, m, n* of the space surrounding the node, and *R* is the gas constant.

5.6. Temperature perturbation

For temperature-perturbation experiments, the initial structures (PDB codes: 2OCJ and 1UOL) were obtained from the stable structures of 20 ns in 300 K. Subsequently, the simulation temperatures were directly increased to 310, 312, 315 and 318 K and simulated in these respective conditions for 5 ns.

Acknowledgments

The research is supported by high-performance computing platform of Northwest A&F University, and is financially supported by the National Natural Science Foundations of China (Grant Nos. 10801025 and 31170796) and the Youth Scientist Fund of NWSUAF.

Appendix A. Supplementary data

Supplementary data associated with this article can be found, in the online version, at doi:10.1016/j.jsb.2011.12.008.

References

Levy, Y., Onuchic, J., 2006. Water mediation in protein folding, molecular recognition. Annu. Rev. Biophys. Biomol. Struct. 35, 389–415.

Vogelstein, B., Lane, D., Levine, A.J., 2000. Surfing the p53 network. Nature 408, 307–310.

Ishimaru, D., Ano Bom, A.P.D., Lima, L.M.T.R., Quesado, P.A., Oyama, M.F.C., de Moura Gallo, C.V., Cordeiro, Y., Silva, J.L., 2009. Cognate DNA stabilizes the tumor suppressor p53 and prevents misfolding and aggregation. Biochemistry 48 (26), 6126–6135.

Okorokov, A.L., Orlova, E.V., 2009. Structural biology of the p53 tumour suppressor. Curr. Opin. Cell Biol. 19, 197–202.

Khoo, K.H., Joerger, A.C., Freund, S., Fersht, A.R., 2009. Stabilising the DNA-binding domain of p53 by rational design of its hydrophobic core. Protein Eng. Des. Sel. 22 (7), 421–430.

Cañadillas, J.M.P., Tidow, H., Freund, S., Rutherford, T., Ang, H.C., Fersht, A.R., 2006. Solution structure of p53 core domain: structural basis for its instability. Proc. Natl. Acad. Sci. USA 103 (7), 2109–2114.

Vousden, K.H., Lu, X., 2002. Live or let die: the cell's response to p53. Nat. Rev. Cancer 2, 594–604.

Silva, J.L., Vieira, T.C.R.G., Gomes, M.P.B., Bom, A.P.A., Lima, L.M.T.R., Freitas, M.S., Ishimaru, D., Cordeiro, Y., Foguel, D., 2010. Ligand binding, hydration in protein misfolding: Insights from studies of Prion, p53 tumor suppressor proteins. Acc. Chem. Res. 43 (2), 271–279.

Ishimaru, D., Andrade, L.R., Teixeira, L.S.P., Quesado, P.A., Maiolino, L.M., Lopez, P.M., Cordeiro, Y., Costa, L.T., Heckl, W.M., Weissmüller, G., Foguel, D., Silva, J.L., 2003. Fibrillar aggregates of the tumor suppressor p53 core domain. Biochemistry 42, 9022–9027.

Fernández, A., Scheraga, H.A., 2003. Proteins with H-bond packing defects are highly interactive with lipid bilayers: Implications for amyloidogenesis. Proc. Natl. Acad. Sci. USA 100, 113–118.

Fernández, A., Kardos, J., Scott, L.R., Goto, Y., Berry, R.S., 2003. Structural defects, the diagnosis of amyloidogenic propensity. Proc. Natl. Acad. Sci. USA 100, 6446–6451.

Fernández, A., Rogale, K., Scott, R., Scheraga, H.A., 2004. Inhibitor design by wrapping packing defects in HIV-1 proteins. Proc. Natl. Acad. Sci. USA 101, 11640–11645.

Xu, X., Yang, W., Wang, X., Li, Y., Wang, Y., Ai, C., 2011a. Dynamic communication between androgen and coactivator: mutually-induced conformational perturbations in androgen receptor ligand-binding domain. Proteins. 79 (4), 1154–1171.

Xu, X., Wang, X., Xiao, Z., Li, Y., Wang, Y.H., 2011b. Two TPX2-dependent switches control the activity of Aurora A. PLoS One 6 (2), e16757.

Modig, K., Liepinsh, E., Otting, G., Halle, B., 2004. Dynamics of protein, peptide hydration. J. Am. Chem. Soc. 126, 102–114.

De Simone, A., Dodson, G.G., Verma, C.S., Zagari, A., Fraternali, F., 2005. Prion, water: tight, dynamical hydration sites have a key role in structural stability. Proc. Natl. Acad. Sci. USA 102 (21), 7535–7540.

Papoian, G.A., Ulander, J., Eastwood, M.P., Luthey-Schulten, Z., Wolynes, P.G., 2004. Water in protein structure prediction. Proc. Natl. Acad. Sci. USA 101, 3352–3357.

Kitayner, M., Rozenberg, H., Kessler, N., Rabinovich, D., Shaulov, L., Haran, T.E., Shakked, Z., 2006. Structural basis of DNA recognition by p53 tetramers. Mol. Cell 22, 741–753.

Fernández, A., 2004. Keeping dry, crossing membranes. Nat. Biotechnol. 22 (9), 1081–1084.

Basse, N., Kaar, J.L., Settanni, G., Joerger, A.C., Rutherford, T.J., Fersht, A.R., 2010. Toward the rational design of p53-stabilizing drugs: probing the surface of the oncogenic Y220C mutant. Chem. Biol. 17, 46–56.

Cho, Y., Gorina, S., Jeffrey, P.D., Pavletich, N.P., 1994. Crystal structure of a p53 tumor suppressor-DNA complex: understanding tumorigenic mutations. Science 265 (5170), 346–355.

Wasielewski, M., Elstrodt, F., Klijn, J.G.M., Berns, Els.M.J.J., Schutte, M., 2006. Thirteen new p53 gene mutants identified among 41 human breast cancer cell lines. Breast Cancer Res. Treat. 99, 97–101.

Ma, B., Levine, A.J., 2007. Probing potential binding modes of the p53 tetramer to DNA based on the symmetries encoded in p53 response elements. Nucl. Acids Res. 35 (22), 7733–7747.

Zhang, L., Yang, Y., Kao, Y., Wang, L., Zhong, D., 2009. Protein hydration dynamics, molecular mechanism of coupled water-protein fluctuations. J. Am. Chem. Soc. 131, 10677–10691.

Barnas, C., Martel-Planche, G., Furukawa, Y., Hollstein, M., Montesano, R., Hainaut, P., 1997. Inactivation of the p53 protein in cell lines derived from human esophageal cancers. Int. J. Cancer 71 (1), 79–87.

Makarov, V.A., Andrews, B.K., Smith, P.E., Pettitt, B.M., 2000. Residence times of water molecules in the hydration sites of myoglobin. Biophys. J. 79, 2966–2974.

Helms, V., 2007. Protein dynamics tightly connected to the dynamics of surrounding, internal water molecules. Chem. Phys. Chem. 8, 23–33.

Guex, N., Peitsch, M.C., 1997. SWISS-MODEL, the Swiss-Pdb Viewer: an environment for comparative protein modeling. Electrophoresis 18, 2714–2723.

Berendsen, H.J.C., van der Spoel, D., van Drunen, R., 1995. GROMACS: a message-passing parallel molecular dynamics implementation. Comput. Phys. Commun. 91, 43–56.

Daura, X., Mark, A.E., van Gunsteren, W.F., 1998. Reversible peptide folding in solution by molecular dynamics simulation1. J. Comp. Chem. 19, 535–547.

Jorgensen, W.L., Chandrasekhar, J., Madura, J.D., Klein, M.L., 1983. Comparison of simple potential functions for simulating liquid water. J. Chem. Phys. 79, 926–935.

Berendsen, H.J.C., Postma, J.P.M., van Gunsteren, W.F., DiNola, A., Haak, J.R., 1984. Molecular dynamics with coupling to an external bath. J. Chem. Phys. 81, 3684–3690.

Hess, B., Bekker, H., Berendsen, H.J.C., Fraaije, J.G.E., 1997. A linear constraint solver for molecular simulations. J. Comput. Chem. 18, 1463–1472.

Darden, T., York, D., Pedersen, L., 1993. Particle mesh Ewald: an N log (N) method for Ewald sums in large systems. J. Chem. Phys. 98, 10089–10092.

Lounnas, V., Pettitt, B.M., 1994a. Distribution function implied dynamics versus residence times, correlations: solvation shells of myoglobin. Proteins 18, 148–160.

Lounnas, V., Pettitt, B.M.A., 1994b. Connected-cluster of hydration around myoglobin: correlation between molecular dynamics simulations, experiment. Proteins 18, 133–147.

Hamelberg, D., McCammon, J.A., 2004. Standard free energy of releasing a localized water molecule from the binding pockets of proteins: double-decoupling method. J. Am. Chem. Soc. 126, 7683–7689.